Chitosan/Snail slime films as multifunctional platforms for potential biomedical and cosmetic applications: physical and chemical characterization

Jennifer Gubitosa[a], Vito Rizzi[a], Paola Fini[b], Fiorenza Fanelli[c], Teresa Sibillano[d], Nicola Corriero[d], Pinalysa Cosma[a*]*

Due to the pollution problem, the use of more sustainable materials with a reduced environmental impact, spanning across biocompatible and biodegradable polymers, is growing worldwide in many different fields, particularly when referring to applications in Life Sciences. Accordingly, in perspective to develop multifunctional materials for potential cosmetic/biomedical purposes, this work reports the physical and chemical characterization of chitosan-based films blended with Snail Slime, exhibiting antioxidant and sunscreen features. A suitable formulation for preparing free-standing chitosan platforms, mixing low molecular weight chitosan, lactic acid, glycerol, and Snail Slime into an appropriate ratio, is thus described. The results obtained by morphological analysis and ATR-FTIR spectroscopy, XRD, swelling (also when varying pH, ionic strength, and temperature), and WVTR measurements evidence a uniform distribution of Snail Slime inside the chitosan network, forming more compacted structures. At first, the UV-Vis analysis is used to infer the theoretical Sun Protection Factor, suggesting these innovative platforms for preventing sunburn. Then, the antioxidant features are investigated using the ABTS assay, displaying a Snail Slime-mediated and dose-dependent boosted activity.

Introduction

For several years, environmental problems, particularly related to the increased use of plastics, have encouraged the application of greener and more sustainable technologies.[1-12] The development of innovative materials has thus been promoted to find solutions and valid alternatives derived from nature, especially for cosmetic and biomedicine companies.[2] Notably, natural polymers have acquired great interest due to their higher biocompatibility and biodegradability if compared to synthetic ones.[3–5] It is worth considering that although advanced methods for synthesizing the polymers used in smart/intelligent food packaging, construction, medicine, etc., could offer many benefits, their concrete usage is limited due to the high costs typically associated with their industrial production, together with biodegradability concerns. On the other hand, biopolymers could be considered low-cost materials, easily processable at the industrial scale.[13]

In this context, there are biopolymers derived from seafood industries.[14,15] Seafood wastes usually contain a great amount of chitin, from which chitosan (CH), a polysaccharide with fascinating features such as biocompatibility, biodegradability, antitumor, antioxidant properties, and so on, is derived.[16] Not surprisingly, chitosan has been proposed in different forms and for many applications. [16–19] Focusing on biomedicine, among the different properties attributed to chitosan, its ability to accelerate wound healing, reduce blood cholesterol levels, stimulate the immune response system, and be a stronger antioxidant agent, appear particularly relevant.[20] Moreover, hybrid systems constituted of chitosan mixed with functional additives having multiple properties, boosting and/or tuning the chitosan ones, have been studied.[4,5,16,21-27,28-30] As well as, biodegradable, antioxidant, anti-aging, anti-inflammatory, skin cleansing, UV rays protector chitosan-based systems have been successfully investigated for cosmetics purposes.[31–34] Starting from this background that highlights how the research activity devoted to chitosan is still in progress, in this work, to develop sustainable multifunctional platforms for potential biomedical and/or cosmetic applications, hybrid chitosan/Snail Slime (CH-SS) composite films are proposed. Particularly, Snail Slime (SS), was incorporated into chitosan hydrogel to form solid-state functional surfaces. Indeed, SS was selected because it is an active natural ingredient used both in cosmetics and biomedicine, which, thanks to its extraordinary composition, can exhibit, at the same time, different interesting features: adhesive, emollient, moisturizing, lubricating, antioxidant, and wound healing properties.[2,35]

[a.] *Università degli Studi "Aldo Moro" di Bari, Dipartimento di Chimica, Via Orabona, 4- 70126 Bari, Italy.*
[b.] *Consiglio Nazionale delle Ricerche CNR-IPCF, UOS Bari, Via Orabona, 4- 70126 Bari, Italy.*
[c.] *Consiglio Nazionale delle Ricerche, Istituto di Nanotecnologia (CNR-NANOTEC) c/o Dipartimento di Chimica, Università degli Studi "Aldo Moro", Via Orabona, 4 - 70126 Bari, Italy.*
[d.] *Consiglio Nazionale delle Ricerche CNR-IC, UOS Bari, Via Amendola,122/O 70126 Bari, Italy.*

Electronic Supplementary Information (ESI) available: Profilometer analyses; X-ray diffraction analyses; Water Contact Angle analyses. See DOI: 10.1039/x0xx00000x

View Article Online
DOI: 10.1039/D2TB02410B

SS is historically known for the experience of the snail farmers when manipulating the snails because they noticed that their wounds or the small scars were quickly repaired, and their hands' roughness was progressively reduced. This statement was derived from the fact that the secretion of slime by snails is necessary as a defense against several mechanical stresses to which these animals are exposed when moving on certain surfaces having more or less marked roughness.[36] Snail mucus contains a combination of natural ingredients beneficial for human skin, including allantoin and glycolic acid.[36] Interestingly, SS has been recently used also for the green synthesis of gold nanoparticles which, when functionalized with the main components of SS, retained the antioxidants and wound healing features of SS, as demonstrated when performing the *in-vitro* experiments.[2,37] However, to our knowledge, despite the SS's huge use in commercial products (such as cosmetics and pharmaceutics), the number of articles in the available literature[38–43] is still low. And there are even fewer if we refer to the synergistic activity of chitosan and SS.[16,44,45] Thus, this work aims to widen the SS applicability and, for this purpose, a comprehensive investigation of the physical and chemical properties of a CH/SS hybrid films was performed. In particular, a suitable formulation for preparing CH/SS films was presented, and, among the large number of features that these composites should exhibit, the attention was focused on their ability to act as antioxidants and UV protectors, boosting the basic chitosan activity. Work is in progress about the possibility of proposing them as facial beauty masks or multifunctional patches having moisturizing, skin-lightening, and wound-healing properties, extending their applications.

Experimental

Materials and Methods

Chemicals. Low molecular weight chitosan, glycerol (anhydrous, reagent grade, having ≥ 99.5% purity), L-(+) lactic acid 80%, ABTS (2,2-Azino-bis (3-ethylbenzothiazoline-6-sulfonic acid) diammonium salt), $K_2S_2O_8$, tyrosinase (from mushroom lyophilized powder, ≥1000 unit/mg solid), tyrosine (reagent grade, ≥ 98%), NaCl, NaOH, HCl, Perdrogen™ 30% H_2O_2 (w/w), KH_2PO_4, and KOH used to prepare buffer solutions at pH 7.5 were purchased from Sigma-Aldrich (Milan, Italy); 4-thio(20-deoxy)thymidine (S^4TdR) having 99+% purity, was purchased from Carbosynth (Compton, Berkshire, UK). The Snail Slime was received from the Società Agricola Dap, di Francesco Paolo Perrotta & C. S.a.s - via Diego Rapolla, - 85029 Venosa (Potenza, Basilicata, Italy).

Snail slime extraction. *Helix Aspersa Muller*, a gastropod mollusk with a shell of 3.5 cm diameter and a weight of about 15 g, was used to obtain the slime. Ozone gas was used to stimulate the snail slime production, thus avoiding animal stress and damage. More specifically, the snails were placed into a machine where the ozone was nebulized for 1 hour. Then, the slime was collected and micro-filtered. Its analytical composition has already been reported in our previous works.[2,46] In summary, the MALDI (+) FT-ICR MS analysis was performed, evidencing the main presence of amino acids (*i.e.,* threonine, tryptophan, arginine, histidine, asparagine, cysteine, glutamine, proline, glycine, and serine), and sulfur-bearing peptides, particularly glutathione, which showed cysteine units. The presence of fatty acids, carbohydrates, polyphenols, and condensed heterocycles was assessed, along with polar lipids, polyphenols, condensed heterocycles, and nucleotides. Furthermore, allantoin and organic acids, such as acetic, citric, lactic, tartaric, and glycolic acids, were also detected.[2,46]

Design and preparation of Chitosan and Chitosan/Snail Slime blended films. Chitosan films were obtained by modifying the procedure of Rizzi *et al*.[4,14,18,19] and Gubitosa *et al.*[47], as detailed in the following. Low molecular weight chitosan powder was dissolved in 0.8% (v/v) lactic acid aqueous solution to finally obtain a 1% (w/v) chitosan concentration after maintaining it under continuous stirring for 24 h. Glycerol was added as a plasticizing agent at 0.5%. Then, the obtained hydrogel was filtered through a coarse sintered glass filter and degassed for 1 h. After degassing, the chitosan hydrogel was placed into a plastic Petri dish and left in an oven at 60°C for 24 h. Chitosan films were finally obtained (CH film) having a thickness of 1 mm, measured during the profilometer analysis. Similarly, Chitosan/Snail Slime composite films (CH-SS) were prepared by mixing different amounts of SS with chitosan hydrogel at different SS concentrations: 4%, 8%, and 12% (v/v), which will be indicated as CH-SS1, CH-SS2 and CH-SS3 films, respectively.

Determination of the theoretical Sun Protection Factor (SPF). A mathematical expression (**Equation 1**) was used to calculate the theoretical SPF of CH and CH-SS films in the UVB region, employing UV-Vis spectrophotometry[6,37,47]:

$$\boldsymbol{SPF}_{\boldsymbol{Spectrophotometric}} = CF \times \sum_{290}^{320} EE(\lambda) \times I(\lambda) \times Abs(\lambda) \quad (1)$$

Where: EE(λ) = erythemal effect spectrum;
I(λ) = solar intensity spectrum;

Abs(λ) = absorbance of CH and CH-SS-based films in the 290-320 nm wavelengths range;
CF = correction factor (= 10).
Since the values of EE(λ)×I(λ) are constant, they were adoptedfrom the literature.[49]

Swelling measurements. Square-shaped (1cm × 1cm) dried CH, and CH-SS films were accurately weighed (W_0) and placed in 10 mL of water, pH 6, at room temperature (293 K). After 60 seconds, the samples were taken from the solution, dried with filter paper to remove the excess water, and then weighed at time t (W_t). The amount of adsorbed water, expressed as Swelling %, was calculated as follows (**Equation 2**):

$$Swelling\ (\%) = \frac{W_t - W_0}{W_0} \times 100 \quad (2)$$

where W_t and W_0 are the wet and dried film weights, respectively. The swelling % was also calculated in water solutions at different pH values from 2 to 12, in NaCl solutions at concentrations in the range 0.1-1M, and at different temperature values from 278 K to 333 K. A heating magnetic stirrer (Arex, Velp Scientifica) controlled with an MGW Lauda R42/2 digital thermometer was used for the latter purpose.

Water Vapor Transmission Rate (WVTR) measurements. The WVTR of chitosan-based materials was evaluated using a 7002 Water Vapor Permeation Analyzer (Illinois Instruments, Inc. U.S.). The instrument can display the WVTR g/m^2/day, and into the instrument is incorporated a Pb_2O_5 sensor. According to Faraday's Combined Laws of Electrolysis, the electrolytic current is a measure of the rate at which water is electrolyzed. Under equilibrium conditions, this equals the rate at which the Pb_2O_5 film absorbs moisture. Thus, the absolute measure of the moisture in the sample gas is obtained by the gas flow rate through the housing and the current in the cell. The films were stored in the cell at 25 ± 1°C and 90 ± 1% relative humidity (RH) for 24 h.

Determination of ABTS scavenging activity. The procedure described in Rizzi *et al.* [37] and Gubitosa *et al.*[7] was adopted with slight changes. Specifically, ABTS was dissolved in water to obtain a 7mM concentration. ABTS radical cation ($ABTS^{\bullet+}$) was obtained by the reaction of the ABTS stock solution with 500 µL of potassium persulfate (0.6 mg/mL). The mixture was left in the dark at room temperature for 12 h before use. The inhibition studies started from this mixture by diluting the latter solution (1:40) in Phosphate buffered Solution (PBS) 0.1M, pH 7.5, in the presence of appropriate amounts of the samples object of study. For this purpose, CH and CH-SS films were dissolved for 10 minutes in PBS 0.1M, pH 7.5, and then different aliquots of these solutions were tested for the ABTS assay. **Equation 3** was used to infer the % of ABTS bleaching, indicative of the chitosan-based film antioxidant activity:

$$\%\ \boldsymbol{ABTS\ bleaching} = \frac{A_{ABTS} - A_{sample}}{A_{ABTS}} \times 100 \quad (3)$$

where, A_{sample} is the absorbance value at 800 nm of the solution containing ABTS and the mentioned aliquots of solutions from CH and CH-SS after 1 h of incubation time, while A_{ABTS} is the absorbance value of the ABTS solution read at the same wavelength before adding the samples.

Determination of the antioxidant activity in the presence of 4-thiothymidine. 4-thiothymidine (S^4TdR) stock solution having a concentration of 1.0×10^{-3} M was prepared in deionized water and used for performing experiments.
Hydrogen peroxide was chosen as a model oxidative agent. An H_2O_2 solution 5.0×10^{-2} M was prepared. The nucleoside oxidation was progressively monitored by achieving UV-Vis spectroscopic measurements, following the intensity of the absorption band at 337 nm, which collapses in favor of by-products. To evaluate the effect of CH and CH-SS films, they were dissolved in PBS 0.1M, pH 7.5 (in 10 minutes), and then the derived solutions were tested in the presence of H_2O_2 and S^4TdR.

View Article Online
DOI: 10.1039/D2TB02110F

UV-Visible measurements. The UV-Visible absorption spectra were collected using a Varian CARY 5 UV-Vis-NIR spectrophotometer (Varian Inc., now Agilent Technologies Inc., Santa Clara, CA, USA) in the range of 200-800 nm, at a 1 nm/s scan rate. Measurements for solid samples were performed by using an appropriate cell holder.

ATR-FTIR spectroscopic measurements. ATR-FTIR spectra were recorded within the 400–4000 cm^{-1} range by using a Fourier Transform Infrared spectrometer (FTIR Spectrum Two from Perkin Elmer, Waltham, MA, USA), whose resolution was set to 4 cm^{-1}. 16 scans were summed for each acquisition.

Scanning Electron Microscopy (SEM) investigation. The surface morphology of the CH and CH-SS films was investigated using a Zeiss SUPRA™ 40 field emission scanning electron microscope. SEM images were acquired with a conventional Everhart-Thornley detector at a working distance of 3 mm, and electron acceleration voltage of 3.00 kV.

Differential Scanning Calorimetry (DSC). DSC measurements were performed with a Q200 TA Instruments thermal analyzer calibrated with indium as standard. For thermogram acquisition, sample sizes of 5 mg were scanned with a heating rate of 10 °C/min over a temperature range from 25 °C to 190 °C. The dry material was placed in an aluminum cup and hermetically sealed. An empty cup was used as a reference, and runs were performed in triplicate. Samples were analyzed under the continuous flux of dry nitrogen gas (50 mL/min).

Results and discussion

Physical and chemical characterization of Chitosan/Snail Slimeblended films.

The morphological features. Homogeneous yellowish blends were obtained by mixing appropriate amounts of Snail Slime (SS) and chitosan (CH) hydrogel. These mixtures, when let dried in a Petri dish, formed thin films (**Scheme 1**) which, dependingon the added SS amount, were indicated as CH, CH-SS1, CH-SS2, and CH-SS3, containing 0%, 4%, 8%, and 12 % (v/v) of SS, respectively.

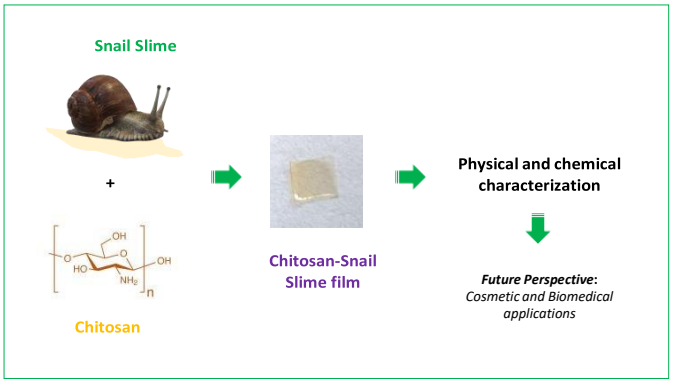

Scheme 1: A cartoon depicting Chitosan/Snail Slime blended films.

These hybrid platforms appeared macroscopically uniform and similar, showing the absence of evident segregation of the blended components (chitosan and SS). This indicated the SS's complete miscibility and homogeneous distribution inside the polymeric film network. The detailed characterization of composite platforms was first subjected to the profilometer analysis (**Figure S1**) to assess this finding. Both CH and CH-SS films were analyzed, and the latter were similar to each other,

despite the added amounts of SS being different. As it can be appreciated from the representative bidimensional white light vertical scanning interferometry images reported in **Figure S1**, the CH and CH-SS films showed similar morphology and good uniform distribution of SS. However, the CH film presented irregular nodules, absent in the case of the CH-SS film. Consequently, the measured route means square roughness of CH film (80 ± 15 nm) was greater than that of the blended one (35 ± 5 nm). So, these outcomes suggested that SS was homogeneously distributed inside CH film, compacting and rearranging its network and leveling the surface. To further confirm the findings, the SEM images were then collected (**Figure 1**). At the micrometric level, cracks and bubbles were absent before (**Figure 1A**) and after SS addition (**Figure 1B**). The films appeared smooth and similar to each other, suggesting how SS was uniformly distributed inside the CH film. Accordingly, the clear absence of a phase separation confirmed the complete miscibility and compatibility of the two interacting components.[48-49]

To infer more information about the effect of SS on CH-film, XRD, DSC, ATR-FTIR, WCA, WVTR, and swelling analyses were subsequently performed.

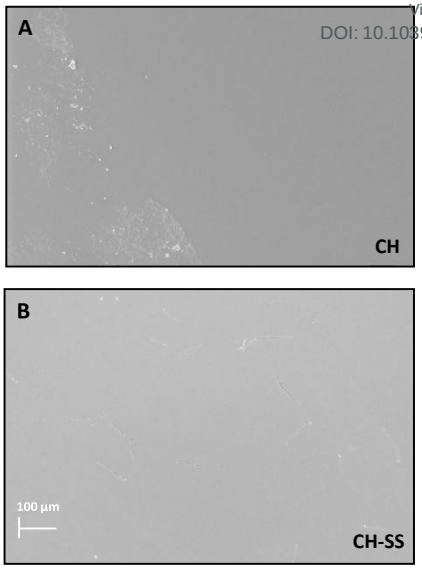

Figure 1: SEM images of CH (**A**) and CH-SS (**B**) films.

XRD and DSC analyses. The crystalline/amorphous nature of the CH and CH-SS films was investigated using the X-ray

diffraction technique. Indeed, it was demonstrated that crystallinity and the amorphous state of chitosan strongly depend on their preparation methods and the presence of additives.[50] X-ray patterns collected on both simple and modified chitosan films (**Figure S2**) evidenced the existence of the amorphous phase for all the investigated samples. Specifically, CH film already had an amorphous character, and the incorporation of SS slightly affected it. In detail, concerning CH film, the incorporation of snail slime increased the amorphous character when passing from CH-SS1 to CH-SS3 films, as demonstrated by the evaluation of the FWHM of the diffraction patterns by the Gaussian fit reported in **Table S1**. Accordingly, as reported elsewhere[48], the presence of SS could perturb the chitosan inter-chain interactions, leading to a loss of structural order.[48] The T_{glass} of chitosan was experimentally determined by DSC measurements. The CH film showed a T_{glass} of 143 °C, and this value was not significantly affected by the presence of SS, indicating that no changes occurred in terms of its amorphous character, although the embedded SS.

ATR-FTIR measurements. The effect of SS in the prepared hybrid films was subsequently studied by performing ATR-FTIR analyses (**Figure 2A**). The results were obtained by comparing the IR vibration modes of the CH film with those obtained from CH-SS films. In the collected ATR-FTIR spectrum of CH film, the main characteristic bands of chitosan were detected[4]: in the 3300-3400 cm^{-1} wavenumber region, the stretching vibration of N-H at 3251 cm^{-1} and O-H at 3376 cm^{-1} were undoubtedly observed; the triplet at 2871/2933/2980 cm^{-1} was attributed to the symmetric and asymmetric C-H stretching; the C=O stretching at 1710 cm^{-1}, and the NH_2 stretching at 1574 cm^{-1} were also registered. The bands observed at 1121 cm^{-1} and 1070 cm^{-1} can be ascribed to the C-O-C asymmetric and symmetric stretching, respectively, with the contribution of the C-O

View Article Online
DOI: 10.1039/D2TB02119F

stretching belonging to the alcoholic moieties at 1024 cm^{-1} (typical for saccharide structures). When the ATR-FTIR spectra referred to CH-SS films were recorded, new signals were detected and undoubtedly attributed to the presence of SS in CH film. Indeed, these characteristic bands were proportional to the amount of added SS and occurred more evident when passing from CH-SS1 to CH-SS3 films. So, the ATR-FTIR spectrum of pure SS was also collected to assess this finding.

The attributions of the ATR-FTIR spectrum of SS were obtained following the literature and the results reported in our previous works,[2,37] in which the analytical profile of the Snail Slime was outlined through the mass spectrometry analysis. More specifically, the bands detected at around 1700 cm^{-1} and 1580 cm^{-1} were related to the amide bonds of peptides and proteins. Likely, the intense absorption peak around 1700 cm^{-1} could also be ascribed to SS's high allantoin and glycolic acid content. The band at about 1390 cm^{-1} arose from carboxylate moieties belonging to the derivatives of sugars and amino acid chains. Indeed, the slight peaks at 1192 cm^{-1} and lower wavenumber values represented the low contribution of O-glycosidic bonds. The peaks at 2850 cm^{-1} and 2930 cm^{-1} were attributed to CH_2 and CH_3 moieties from protein and lipidic components. Finally, the signals in the range 2900-3500 cm^{-1} confirmed the presence of OH and NH moieties. On the other hand, the possible contribution of polyphenols could be retrieved in the range of 1500-1700 cm^{-1}.

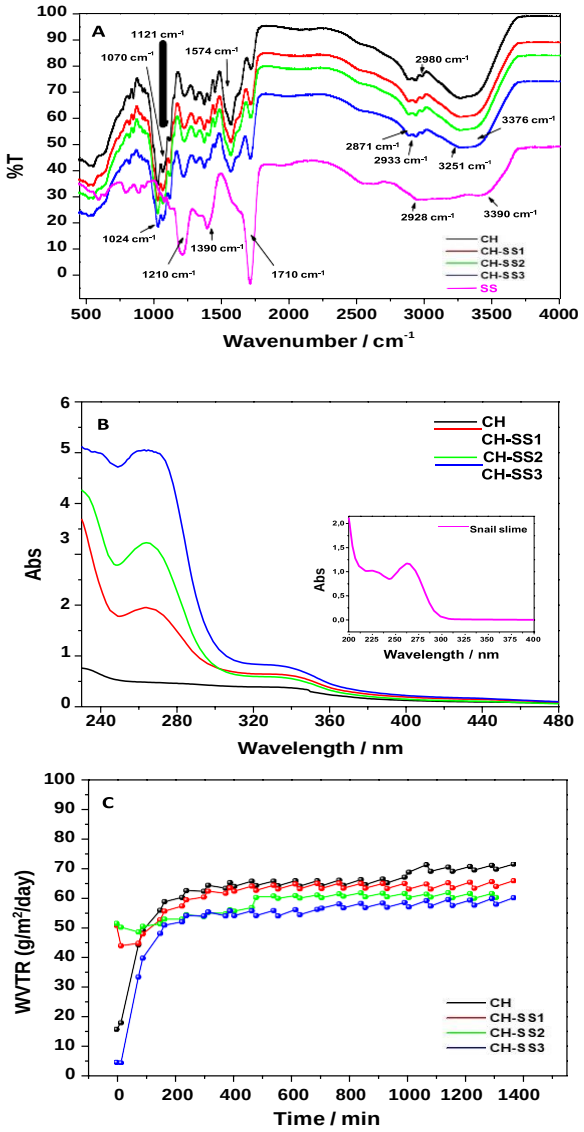

Figure 2: ATR-FTIR (A), UV-Vis (B), and WVTR (C) measurements of CH, CH-SS1, CH-SS2, and CH-SS3 films, containing 0%, 4%, 8%, and 12 % (v/v) of SS, respectively. Inset: UV-Vis absorption spectrum of SS. WVTR analysis reported a standard deviation of 3% to each point, referred to measurements reproduced in triplicate.

On this ground, the contribution of SS signals in the CH film spectrum can be confirmed. Moreover, the addition of SS determined a general broadening of the signals, which tended to assume the SS spectrum's main profile due to the signal's superposition. This behavior was clearly observed in the CH-SS3 film that contained the highest amount of SS (**Figure 2A**). The SS signals in the region between 1500-1700 cm^{-1} strongly contributed to the CH film spectrum, and particularly the band at 1710 cm^{-1} occurred significantly evident. To the same extent, the bands at 1200-1450 cm^{-1} were also affected by the SS. However, although SS was present in CH film and its contribution was clearly evidenced, the signals in the range 2900-3500 cm^{-1} attributed to -OH and -NH moieties of the main components of SS, *i.e.*, peptides and proteins did not show a strong relevance as observed for other spectrum regions.

According to other similar works[17,51] the findings could be attributed to the involvement of SS main components in the interaction with chitosan, taking into account H-bonds and electrostatic interaction.

UV-Vis measurements. Interestingly, other information between CH and CH-SS films was obtained from the UV-Vis investigation. The UV-Vis absorption spectra of CH and CH-SS blended films were collected and are reported in **Figure 2B**. If CH film showed a low absorption in the UV-Vis range, on the other hand, the CH-SS films exhibited, below 300 nm, an absorbance increase that appeared to be correlated with the increased amount of the added SS. For the sake of comparison, the *inset* in **Figure 2B** reports the UV-Vis spectrum of diluted SS, indicating that the main absorption of SS, associated with its main components,[46] was also retained when blended with chitosan.

This high absorption in the UV-Vis spectrum region, particularly starting below 400 nm, should be considered an interesting and positive feature of these films, especially concerning cosmetics and biomedicine applications.[33] Indeed, referring to CH-SS, the presence of SS could boost UV protection, potentially preventing sunburns, as already assessed in our previous study.[37] Skin photodamage is usually associated with both the UV-induced production of Reactive Oxygen Species (ROS) and the inactivation of Nuclear factor erythroid 2-related factor-2 (Nrf2). If the ROS are over-produced after the UV rays exposition, the Nrf2 is inactivated by modifying the pathway of the Nrf2/antioxidant response element-mediated system. So, the antioxidant defense system is affected, promoting the onset of skin problems.[52,53]

On this ground, the latter diseases could be potentially prevented by the proposed films and, using the theoretical approach explained in our previous works,[37] the SPF values were calculated for each composite film to quantify the protection ability from the UV sunlight. In detail, by means of **Equation 1**, the following SPFs were inferred when passing from CH to CH-SS films: 6 for CH and 25, 40, and 60 for CH-SS1, CH-SS2, and CH-SS3 films, respectively. These high values indicated the potential strong ability of the proposed films to protect the skin from UV rays, presenting a novel strategy to prevent photodamage.

Water Vapor Transmission Rate (WVTR) and Water Contact Angle (WCA) analyses. WVTR and WCA analyses were performed to deeply investigate the CH and CH-SS film moisturizing and wettability features. As well known, the mechanism of WVTR is a diffusive process in which water vapor condenses and dissolves on a certain surface, and the liquid water diffuses inside.[54] According to the previous literature related to chitosan films,[17,54] the increased mobility of the polymer chains usually is a condition that favors WVTR through the film. So, it means that the moisture could easily penetrate the hydrophilic domains of chitosan according to the polymer assemblies. Furthermore, another aspect that should be considered is related to protonated amino groups present on chitosan chains that affect the network arrangement.[4] Indeed, the higher the protonation degree, the higher the polar character of chitosan, favouring the water diffusion and the swelling due to the higher electrostatic repulsion between polymer chains.[55,56] As reported in **Figure 2C**, the addition of SS to chitosan film perturbed the chitosan network. So, CH-SS films showed slightly lower WVTR values, denoting slightly less hydrophilic structures.

In detail, the WVTR values of CH and CH-SS films were high, but a SS dose-dependent trend was observed: from CH to CH-SS3 films, the WVTR significantly decreased by increasing the SS content (measurements were performed in triplicate with a standard deviation of 3%). So, it was possible to assess the formation of more condensed networks attributed to the SS presence. Particularly, chitosan hydroxyl and amino moieties could be involved in forming H-bonds and coulombian interaction with SS hindering the polymer chains' movement by reducing the water transmission.[54] Based on these considerations, it is possible to hypothesize that the CH-SS films could behave like potential skin moisturizers. This is a well-known feature of chitosan films in cosmetics and/or biomedicine applications, showing both moisture-absorption and moisture-retention ability.[30,33,57] In particular, the low WVTR of chitosan films blended with snail slime makes these films more suitable as skin moisture-retention systems.

In this regard, wettability can be considered a fundamental surface property, particularly if referring to polymeric films for cosmetic applications. So, the contact angle measurements were additionally performed to confirm these results. Wettability studies usually involve the measurement of contact angles as the primary data, which indicates the degree of wetting when a solid and liquid interact.[58] Once again, CH and CH-SS were compared, and the films with different SS content appeared similar to each other. So, for comparison, the general indication of CH-SS is reported. **Figure S3** shows the time-lapse images. The water contact angle, evaluated as soon as the water droplet was deposited on the films, was 65 ± 4° and 77 ± 4° for the CH and the CH-SS films, respectively. This suggested that the presence of the SS slightly reduced the wettability of the CH-based films, in excellent agreement with the WVTR analysis. In addition, as can be appreciated in **Figure S3**, the water droplets deposited on the samples apparently inflate over time due to film swelling. Interestingly, this swelling phenomenon seemed to be slightly slower and less pronounced in the case of the blended CH-SS film. In this regard, the swelling measurements were performed to investigate this evidence and to assess the behavior of CH-SS when swelled in water by changing different parameters.

Swelling measurements.

As a first step, by fixing the solution pH values, i.e., 6, at room temperature, the comparison between the CH and CH-SS films was considered, and the % of swelling in water was calculated after a short contact time, 60 seconds, to avoid the dissolution of the films. Indeed, it is worth highlighting that long-time exposure of these films to water favored their complete dissolution. **Equation 2** was used to infer the % of swelling. The

camera pictures reported in **Figure 3A** show how chitosan films appeared after the swelling in water for 60 seconds and subsequently after the re-drying process. As can be observed, the size of the reported film largely increased after the contact with water, and the process was not reversible. Indeed, the films remained larger after the drying process compared to the corresponding ones before the water contact.

Differences in % of swelling were detected between the CH and composite films during the first time of exposure to water, and the results are reported in **Figure 3B**. In excellent agreement with the previous discussion, the swelling % was dramatically reduced by passing from CH to CH-SS films, with the lowest value registered in the presence of the highest amount of SS (CH-SS3 film). In particular, the observed swelling values were quite high and SS dose-dependent by passing from 1000 % for CH to 300 % for CH-SS3 film. Hence, the presence of SS reduced the diffusion of water molecules into the films that in turn could differently relax the chitosan structure due to the association/dissociation of hydrogen bonding between the amino moieties inside the polymeric network.[51,59-63] Specifically, the swelling phenomenon is a complex process involving at first the diffusion of water molecules into the polymer network, then the relaxation of hydrated polymer chains, and at the end, the polymer network expansion.[60] According to the literature[61], since the experiments of swelling were performed below the chitosan T_{glass}, experimentally evaluated at 143°C, the water diffusion rate could be faster than the polymer relaxation rate or can be about the same order of magnitude. However, the amount and types of additives in chitosan assembly could limit the macromolecular chain relaxation.[60] Therefore, when CH was in the presence of SS, the latter rearranged the chitosan assembly by packing its domains, reducing the migration of water molecules, rendering the film less hydrophilic.[17,61-63] Moreover, it is worth mentioning that chitosan's swelling depends on the protonation degree of NH moieties. Indeed, positive charges would enhance the repulsion, favoring the swelling.[4] On the other hand, if these charges are balanced, reducing their contribution, the chitosan structure becomes more rigid, hindering water diffusion and swelling. On this ground, it is possible to confirm that SS main components interacted with chitosan chains also through electrostatic interaction, further reducing the film swelling.

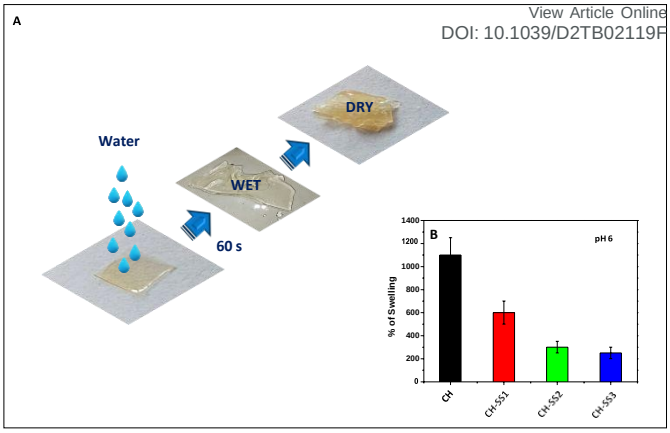

Figure 3: A cartoon depicting a chitosan-based film appearing after contact with water (**A**) and a graph reporting the % of swelling related to CH, CH-SS1, CH-SS2, and CH-SS3 films (**B**).

To further investigate the features of the hybrid films, the swelling measurements were subsequently performed under extreme work conditions, evaluating the role of temperature, pH, and ionic strength.

Effect of temperature on the swelling degree. The CH and CH-SS films were swelled in water with different temperature values ranging from 278 to 333K, evaluating the behavior at 310K (physiological temperature).

The experiments were performed in a large range of temperatures to obtain additional information to confirm further the findings reported in the paper about the role of SS when present in CH films.

Again, 60 seconds were adopted as the reference contact time. The results reported in **Figure 4** indicate that all the films showed a temperature-responsive swelling behavior.

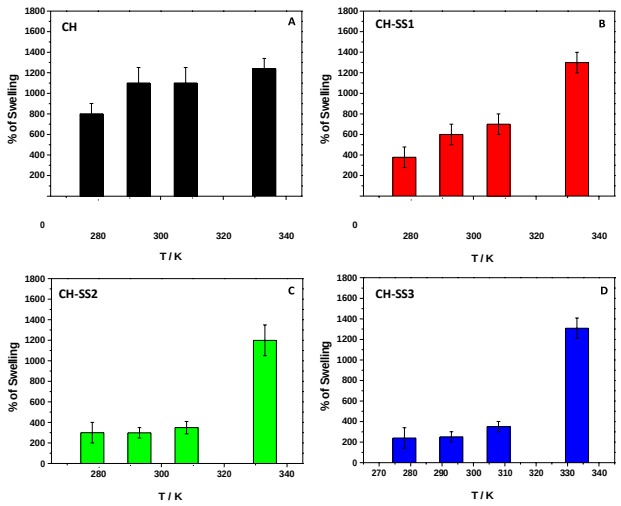

Figure 4: % of swelling related to CH (**A**), CH-SS1 (**B**), CH-SS2 (**C**), and CH-SS3 (**D**) films when immersed in water at different temperatures.

In particular, for the CH film (**Figure 4A**), the effect was gradual. While, for CH-SS films, the swelling degree changed significantly

only at the highest adopted temperature (**Figures 4 B-D**), and the effect was more pronounced for CH-SS2 and CH-SS3 when the amount of SS was increased. So, the findings evidenced that, for CH film, the increase in temperature favored the chitosan chain relaxation, creating more space for water by increasing the swelling. On the other hand, the presence of SS hindered the water diffusion due to the more compacted assemblies, and the films largely swelled only at higher temperature values.

Effect of pH and ionic strength on the swelling degree. The swelling behavior of the CH and CH-SS films by varying the pH values was investigated after preparing different water solutions having pH values ranging from 2 to 12 (**Figure 5**).

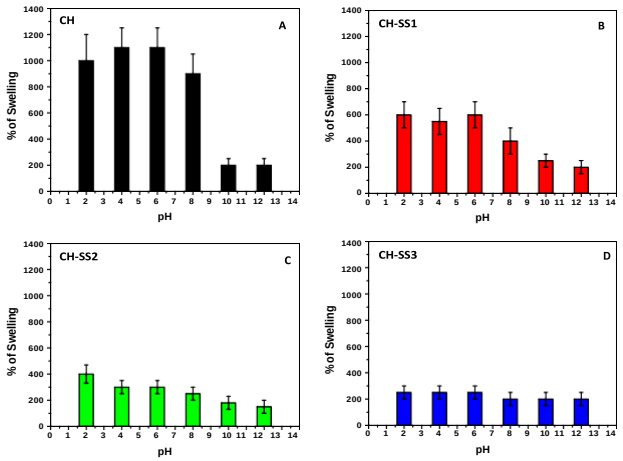

Figure 5: % of swelling related to CH (**A**), CH-SS1 (**B**), CH-SS2 (**C**), and CH-SS3 (**D**) films when immersed in water at different pH values.

If CH film without SS occurred greatly affected by the pH (**Figure 5A**), on the other hand, the presence of SS tended once again to reduce the effect. This behavior could be rationalized by considering the previous discussion about the role of protonated amino groups and the interactions between chitosan and SS. In general, -NH_2 groups in the chitosan chains can interact with the hydrogen ions (H^+), forming ammonium-protonated groups. Indeed, chitosan is a weak polybase, and, as

suggested by Rizzi *et al.*,[4] the ionization of amino groups is affected by varying the medium pH values, and it decreases when the pH of the solution increases. In particular, chitosan has a pK_a between 6 and 7[60]; consequently, the amino groups are partially not-protonated at higher pH values. Therefore, at low pH values, positively charged chitosan chains repelled each other by inducing the expansion of the polymer network,

favoring the swelling. Instead, when the water solution pH increases (pH>8), the ionization degree of chitosan decreases,

and the repulsion is expected to be reduced, determining a more compact chitosan assembly with a reduced swelling degree.[4] This is the behavior observed during this work when referring to the CH film (**Figure 5A**).

On the other hand, the results obtained from CH-SS seemed to confirm the compacted structure of the composite film (**Figures 5B-D**) in which the SS components interacted with chitosan through H-bonds and electrostatic interaction: the higher the SS amount, the less the pH effect on the swelling due to the packing of chitosan chains and the screening of charges SS-mediated. Accordingly, the obtained results provided CH-SS films less affected by pH changes, having a lower % of swelling. The effect was more evident in the case of CH-SS2 and 3, when SS was larger.

Some experiments were performed in the presence of salts, to confirm the finding. For this purpose, NaCl was adopted as a model electrolyte (**Figure 6**). **Figures 6A-D** reported the % swelling as a function of salt concentration for all the investigated films. It is evident how the CH film was more affected by the salt concentration, reducing its swelling degree as a function of NaCl amount (**Figure 6A**) than the CH-SS composite films that appeared less affected, especially by increasing the amount of SS (**Figure 6B-D**).

This data confirmed as the charges on the polymer backbone played an essential role during the swelling mechanism: if the electrostatic repulsion enhanced the polymer structure expansions, on the other hand, the presence of electrolytes neutralized the charges of the polymer, reducing the swelling degree. Furthermore, the osmosis contribution to water permeation should be considered, favoring the chitosan film's shrinkage.[57-59] In detail, due to the intrinsic charges of the chitosan polymer, the swelling and shrinking of a film can be affected by the ratio between the concentration of free ions inside and outside the film: if the ions' amount inside the film is lower than that in the solution, the film tends to shrink under the effect of the osmotic pressure in the surrounding. Alternatively, the film swells due to a large internal osmotic pressure.[66,67]

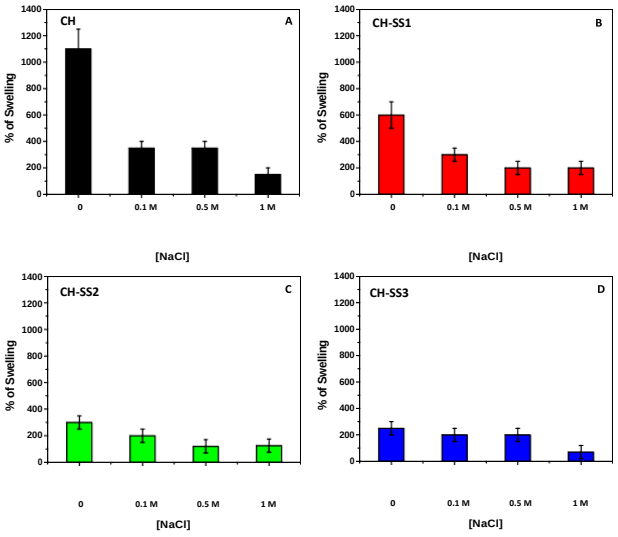

Figure 6: % of swelling related to CH (**A**), CH-SS1 (**B**), CH-SS2 (**C**), and CH-SS3 (**D**) films when immersed in water at different NaCl concentrations.

Therefore, by increasing the concentration of NaCl, the external osmotic pressure raised, and the swelling of film decreased. In contrast, the internal osmotic pressure of the films did not change, also due to the SS components that compacting the

assembly.[67–70] This effect was particularly noticeable when the concentration of the salt was 1 M.

Antioxidants features

ABTS assay. The antioxidant activity was evaluated by performing the ABTS assay following the discoloration of the solutions object of study. More specifically, CH and CH-SS films were previously swelled in water buffered (PBS 0.1 M) at pH 7.5 for 10 minutes (time necessary to dissolve the films completely). Subsequently, the derived solutions were subjected to the ABTS assay. To compare the activity of each film, 100 µL of these water solutions were diluted in 900 µL of PBS, 0.1 M, pH 7.5, in the presence of ABTS, and the bleaching of the latter was spectrophotometrically monitored after 1 h adopted as incubation time.

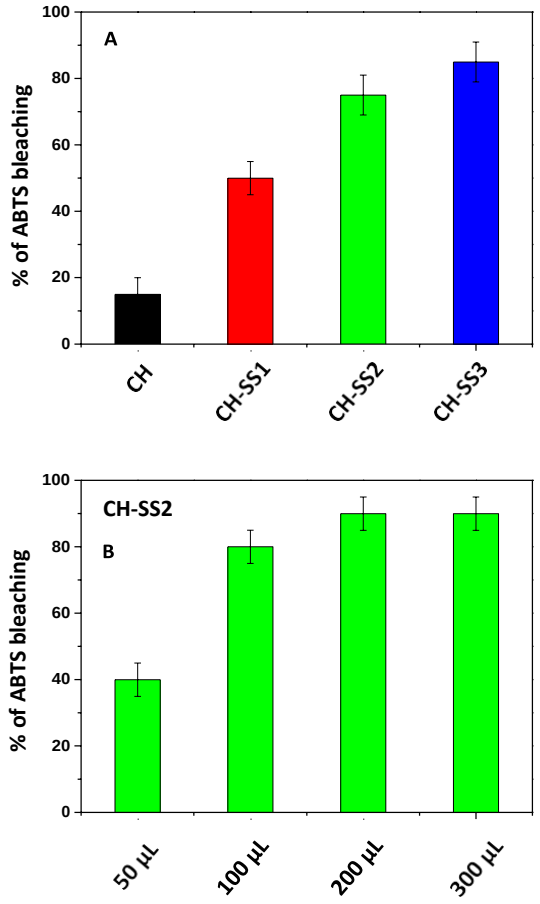

Figure 7: % of ABTS bleaching when in the presence of dissolved CH, CH-SS1, CH-SS2, and CH-SS3 films (**A**) in PBS. 100 µL of the derived solutions were subjected to the ABTS assay; the % of ABTS bleaching in the presence of dissolved CH-SS2 in PBS was calculated, and then different aliquots of these water-based solutions were subjected to the ABTS assay (**B**).

By comparing the obtained results, reported in **Figure 7A**, a clear dose-dependent effect of the added SS can be observed. If in the presence of the dissolved CH film, the lowest ABTS bleaching was observed; on the other hand, the dissolution of CH-SS films boosted the action, rapidly discoloring the solution and increasing the ABTS degradation. Indeed, as reported in the literature,[71] chitosan has an intrinsic antioxidant power that could be improved thanks to the addition of some functional additives. In particular, the snail slime contribution can be evidenced by passing from CH-SS1 to CH-SS3 films when the % of ABTS bleaching increased up to 90%. To further investigate these findings, the CH-SS2 film was selected, and the ABTS assay was performed by using different aliquots (50 µL, 100 µL, 200 µL, and 300 µL) of the solution in which the film was previously dissolved, following the same procedure described before. **Figure 7B** reports the obtained results. By increasing the amount of the tested aliquots, the % of ABTS degradation increased, confirming the dose-effect and the role of SS. So, the proposed hybrid films, thanks to the antioxidant activity of SS, as already evidenced by Rizzi *et al*.,[37] boosted the chitosan property, and they can be proposed as powerful antioxidant platforms potentially able to fight skin stress, skin aging, and all the processes related to ROS overproduction.

View Article Online
DOI: 10.1039/D2TB02410E

Antioxidant test: CH-SS film for preventing 4-thiothymidine oxidation H_2O_2-mediated.

To further confirm the antioxidant features of the studied films, preserving, for example, the oxidation of biomolecules, the modified nucleoside 4-thiothymidine (S^4TdR) was used for this purpose like a chemical probe, because it is prone to be oxidized by ROS.[72] So, the ability of CH-SS films to prevent its degradation was evaluated. Since S^4TdR, due to its extreme reactivity, was previously proposed as a suitable probe to detect, among various ROS, H_2O_2; this latter was adopted as a powerful oxidant agent.[73] UV–Vis spectroscopy monitored the nucleoside degradation to infer information about the CH and CH-SS films antioxidant ability in scavenging H_2O_2. An S^4TdR solution of 1.0×10^{-3} M in the presence of H_2O_2 5.0×10^{-2} M was used to perform the experiments. As described by Rizzi *et al.*,[72] nucleoside oxidation can be monitored by following the intensity of the absorption band at 337 nm, which collapses in favor of by-products. Once again, experiments were performed in buffered aqueous solutions, pH 7.5, 0.1 M, in presence of 50µL of the solutions in which CH and CH-SS films were previously dissolved. So, the reported UV-Vis spectra are referred to the S^4TdR oxidation H_2O_2-mediated, in which its derived by-products were mainly detected in absence (control), and in presence of dissolved CH-SS1, CH-SS2, CH-SS3 films.

When H_2O_2 oxidizes S^4TdR, several products are expected, and, among the others, thymidine (TdR) and a hydroxylated intermediate (R-SOH) are worth to be mentioned. If TdR shows an absorption band in the UV–Vis spectrum around 265 nm, R-SOH can be evidenced by looking at the absorption at 360 nm. In detail, the TdR formation is induced by the R-SOH hydrolysis.

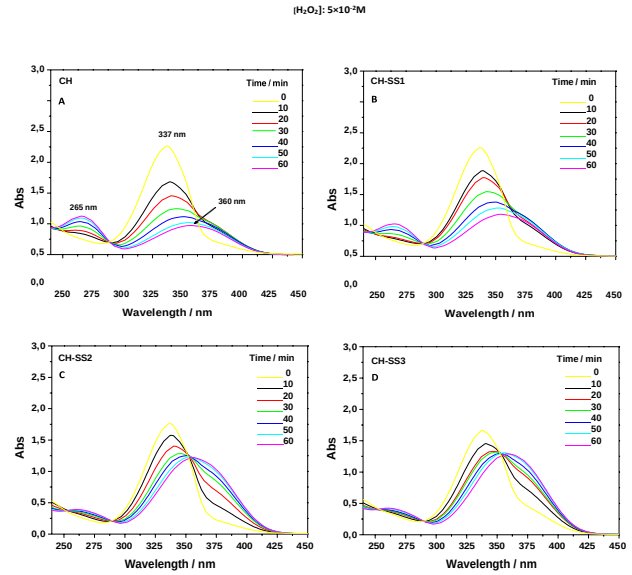

Figure 8: Time evolution of UV-Vis absorption spectra of S^{4}TdR, evidencing the antioxidant role of CH (**A**), CH-SS1 (**B**), CH-SS2 (**C**), and CH-SS3 (**D**) in the presence of H_2O_2.

Starting from the reaction followed in the presence of the CH film (**Figure 8A**), after the first 10 min, a shoulder was observed at 360 nm, indicating the outcoming formation of R-SOH. Accordingly, its contribution can also be highlighted by observing the redshift of the S^{4}TdR main absorption band at 337 nm due to the influence of the species absorbing at 360 nm. By extending the reaction time, these features were better evidenced, and, at the same time, the R-SOH started its hydrolysis/consumption in favor of TdR, which was detected at 265 nm. Significant differences were observed regarding UV-Vis spectra time evolution when the same reaction was performed in the presence of the solutions derived from CH-SS films (**Figure 8B-D**). At first, both S^{4}TdR and R-SOH degradation were slowed down, and the latter's formation was observed with its high contribution, denoting the H_2O_2 scavenging. Accordingly, the TdR formation was slightly observed, especially in the presence of the solution derived from CH-SS2 and CH-SS3 films. The findings indicated that the S^{4}TdR degradation was prevented, retarding its oxidation to TdR, which is the end-oxidation by-product.

Cost evaluations, future directions, and potential applications.

The approximate total cost of the studied films was evaluated by considering the single components used for preparing the blends. For the sake of comparison, the cost associated with a square size of 1 cm × 1 cm film was considered. The following costs were calculated when using commercial chitosan, glycerol, lactic acid, and SS: 380 € for 250 g of chitosan, 178 € for 1L of glycerol, 220 € for 10 g of lactic acid, and 1000 € for 1L of SS, respectively. So, without considering the costs associated with water consumption, the supposed costs associated with a small piece (1 cm × 1 cm) of CH and CH-SS films are the following:

CH films ≅1.40 €;

CH-SS films range from ≅ 1.65 € for CH-SS1, to 2.15 € for CH-SS3.

DOI: 10.1039/D2TB02119F

It should be noted that the main cost is associated with lactic acid.

So, the proposed platforms should be available for daily life applications and can be considered relatively cheap for consumers and industry. Indeed, this work would present the physical and chemical characterization of chitosan-based films in perspective to use them in cosmetic and biomedical fields, for example, as multifunctional facial masks or patches. In this regard, consumers prefer naturally derived bio-polymer hydrogel masks and patches due to their fast biodegradability, thus growing the tendency for more sustainable and biodegradable cosmetic formulations, particularly marketed in these last decades.

Consequently, many worldwide cosmetic companies have proposed a wide range of alternatives. So, the proposed films would be possible candidates to be used in sustainable multifunctional cosmetic/biomedical treatments, not only as antioxidants and UV protectors but also as moisturizing, skin-lightening, and wound-healing agents.

Conclusions

In this work, with the aim to study novel, functional materials for cosmetic and biomedical applications, a preliminary physical and chemical characterization of composite chitosan-based films in blend with Snail Slime added at different % (v/v) was presented. A modified protocol for preparing chitosan hydrogel to obtain free-standing films was thus described. Furthermore, a comprehensive investigation of these platforms was obtained using different synergy techniques. In detail, the morphological analysis showed the uniform distribution of the snail slime inside chitosan films, forming compacted domains without cracks; the affinity between the two components was evidenced.

ATR-FTIR, WCA, WVTR, DSC, XRD, surface roughness, and swelling measurements corroborated the findings. The effect of pH, ionic strength, and temperature on swelling was also evaluated. The results showed that if, on the one hand, the swelling of chitosan film was largely affected when the listed parameters were varied, on the other hand, the hybrid platforms in the presence of the snail mucus appeared less responsive due to the compacted chitosan network.

Employing UV-Vis spectroscopy, among the possible properties, the theoretical SPF was also inferred, demonstrating as the blends could potentially act as sunscreens, preventing sunburns. Additionally, the antioxidant features were spectrophotometrically investigated through the ABTS assay, which showed as the % of ABTS bleaching increased from CH to CH-SS3 films due to the boosted effect of the snail slime. Accordingly, the results were further confirmed by monitoring the protective role of the hybrid platforms towards the oxidation of a sulphur nucleoside, the 4-thiotymidine. Indeed, the films were able to delay the degradation of this biomolecule in presence of H_2O_2, selected as model ROS. Novel horizons are thus opened for the use of these hybrid platforms that

represent the starting point to tune other properties useful in biomedicine and cosmetics for realizing less expensive multifunctional platforms.

Author Contributions

Vito Rizzi: Conceptualization, validation, methodology, writing—review, and editing; **Jennifer Gubitosa**: Conceptualization, validation, investigation, writing—original draft preparation; **Nicola Corriero and Teresa Sibillano**: XRD experiments; **Paola Fini**: validation, Data curation; **Fiorenza Fanelli:** WCA and Profilometer analyses; **Pinalysa Cosma**: formal analysis, resources, project administration, writing—review and editing, funding acquisition.

Conflicts of interest

There are no conflicts to declare.

Acknowledgements

This work was supported by the follwing projects: “Research for Innovation (REFIN) per l’individuazione dei progetti di ricerca” – PUGLIA FESR-FSE 2014/2020, Project title: “Incontro tra Ricerca & Impresa per lo Sviluppo Sostenibile del territorio (IRISS): valorizzazione di scarti alimentari per la rimozione di contaminati emergenti dalle acque”; “Dottorati di ricerca in Puglia XXXIII, XXXIV, XXXV ciclo, POR PUGLIA FESR-FSE 2014/2020”; Horizon Europe Seeds, Project title: “Gestione sostenibile di scarti Agroalimentari come fonte Innovativa di biomateriali multifunzionali per la salute umana e l’Ambiente (G.A.I.A)”. We gratefully acknowledge Prof. Elisabetta Fanizza, Department of Chemistry, University of Bari “Aldo Moro”, Italy, for the SEM analyses; Mr. Savino Cosmai from CNR NANOTEC (CNR Institute of Nanotechnology), Bari, Italy, for performing the WVTR measurements; Francesco Paolo Perrotta and Francesca D’Andretta, Società Agricola Dap di Francesco Paolo Perrotta & C. S.a.s - via Diego Rapolla, - 85029 Venosa (Potenza, Basilicata, Italy), as snail slime suppliers.

Notes and references

1 J. K. Saxe, L. Hoffman and R. Labib, *Green Chem.*, 2022, **24**, 4969–4980.

2 J. Gubitosa, V. Rizzi, P. Fini, A. Laurenzana, G. Fibbi, C. Veiga-Villauriz, F. Fanelli, F. Fracassi, A. Onzo, G. Bianco, C. Gaeta, A. Guerrieri and P. Cosma, *Soft Matter*, 2020, **16**, 10876-10888. DOI:10.1039/D0SM01638A.

3 F. Ahmadi, Z. Oveisi, S. Mohammadi Samani and Z. Amoozgar, *Res. Pharm. Sci.*, 2015, **10**, 1–16.

4 V. Rizzi, P. Fini, F. Fanelli, T. Placido, P. Semeraro, T. Sibillano, A. Fraix, S. Sortino, A. Agostiano, C. Giannini and P. Cosma, *Food Hydrocoll.*, 2016, **58**, 98-112. DOI:10.1016/j.foodhyd.2016.02.012.

5 S. V. G. Kumari, K. Pakshirajan, G. Pugazhenthi, International Journal of Biological Macromolecules, 2022, **221**, 163–182.

6 F. Baghi, A. Gharsallaoui, E. Dumas, S. Ghnimi *Foods* 2022, **11(5)**, 760.

7 J. Gubitosa, V. Rizzi, P. Fini, R. Del Sole, A. Lopedota, V. Laquintana, N. Denora, A. Agostiano and P. Cosma, *Mater. Sci. Eng. C*, 2020, **106**, 110170.

8 S. Jafarzadeh, A. M.Nafchi, A. Salehabadi, N. Oladzad-Abbasabadi, S. M. Jafari, *Advances in Colloid and Interface Science*, 2021, **291**, 102405.

9 D. Daniloski, A. T. Petkoska, N. A. Lee, A. El-Din Bekhit, A. Carne, R. Vaskoska, T. Vasiljevic, *Trends in Food Science & Technology* 2021, **111**, 688.

10 A.T. Petkoska, D. Daniloski, N. M. D’Cunha, N. Naumovski, A. T. Broach, *Food Research International* 2021, **140**, 109981.

11 R. Ouétchéhou, D. S. Dabadé, G. Vieira-Dalodé, A. F. Sanoussi, A. B. Fagla-Amoussou, M. H. Hounhouigan, D. J. Hounhouigan, P. Azokpota, *Afr. J. Food Sci.*, 2022, **15(4)**, 131.

12 R. Gheorghita, G. Gutt, S. Amariei, Coatings 2020, 10, 166;

13 V. Rizzi, J. Gubitosa, P. Fini, R. Romita, S. Nuzzo and P. Cosma, *Materials (Basel).*, 2019, **12**, 3810.

14 M. Yadav, P. Goswami, K. Paritosh, M. Kumar, N. Pareek and V. Vivekanand, *Bioresour. Bioprocess.*, 2019, **6**, 8.

15 V. P. Santos, N. S. S. Marques, P. C. S. V Maia, M. A. Lima, L. D. Franco and G. M. Campos-Takaki, *Int. J. Mol. Sci.*, 2020, **21**, 4290.

16 M. F. Di Filippo, S. Panzavolta, B. Albertini, F. Bonvicini, G. A. Gentilomi, R. Orlacchio, N. Passerini, A. Bigi and L. S. Dolci, *Int. J. Biol. Macromol.*, 2020, **143**, 126–135.

17 V. Rizzi, J. Gubitosa, P. Fini, R. Romita, S. Nuzzo, J. A. Gabaldón, M. I. F. Gorbe, T. Gómez-Morte and P. Cosma, *J. Environ. Sci. Heal. Part A*, 2021, **56**, 145–156.

18 V. Rizzi, F. Romanazzi, J. Gubitosa, P. Fini, R. Romita, A. Agostiano, A. Petrella and P. Cosma, *Biomolecules*, 2019, **9**, 571.

19 E. Talón, K. T. Trifkovic, V. A. Nedovic, B. M. Bugarski, M. Vargas, A. Chiralt and C. González-Martínez, *Carbohydr. Polym.*, 2017, **157**, 1153–1161.

20 W. Wang, Q. Meng, Q. Li, J. Liu, M. Zhou, Z. Jin and K. Zhao, *Int. J. Mol. Sci.*, 2020, **21**, 487.

21 D. Zhao, S. Yu, B. Sun, S. Gao, S. Guo and K. Zhao, *Polym.*, 2018, **10**, 462.

22 F. Croisier and C. Jérôme, *Eur. Polym. J.*, 2013, **49**, 780–792.

23 N. Nady and S. H. Kandil, *Membr.*, 2018, **8**, 2.

24 C. S. Cunha, P. J. Castro, S. C. Sousa, R. C. Pullar, D. M. Tobaldi, C. Piccirillo and M. M. Pintado, *Int. J. Biol. Macromol.*, 2020, **159**, 1177–1185.

25 M. Kouhi, M. P. Prabhakaran and S. Ramakrishna, *Trends Food Sci. Technol.*, 2020, **103**, 248–263.

26 M. A. López-Mata, S. Ruiz-Cruz, N. P. Silva-Beltrán, J. de J. Ornelas-Paz, V. M. Ocaño-Higuera, F. Rodríguez-Félix, L. A. Cira-Chávez, C. L. Del-Toro-Sánchez and K. Shirai, *Int. J. Polym. Sci.*, 2015, **2015**, 974506.

27 X. Song, L. Liu, X. Wu, Y. Liu and J. Yuan, *Int. J. Mol. Sci.* , 2021, **22**, 7769.

28 P. Cazón, A. Antoniewska, J. Rutkowska and M. Vázquez,

Int. J. Biol. Macromol., 2021, **186**, 365–376.

29 M. Moradi, H. Tajik, S. M. Razavi Rohani, A. R. Oromiehie, H. Malekinejad, J. Aliakbarlu and M. Hadian, *LWT - Food Sci. Technol.*, 2012, **46**, 477–484.

30 C. R. Afonso, R. S. Hirano, A. L. Gaspar, E. G. L. Chagas, R. A. Carvalho, F. V. Silva, G. R. Leonardi, P. S. Lopes, C. F. Silva and C. M. P. Yoshida, *Int. J. Biol. Macromol.*, 2019, **132**, 1262–1273.

31 L. Panariello, A. Vannozzi, P. Morganti, M.-B. Coltelli and A. Lazzeri, *Cosmet.*, 2021, **8**, 27.

32 C. Casadidio, D. V Peregrina, M. R. Gigliobianco, S. Deng, R. Censi and P. Di Martino, *Mar. Drugs*, 2019, **17**, 369.

33 I. Aranaz, N. Acosta, C. Civera, B. Elorza, J. Mingo, C. Castro, M. D. Gandía and A. Heras Caballero, *Polym.*, 2018, **10**, 213.

34 Q. Ta, J. Ting, S. Harwood, N. Browning, A. Simm, K. Ross, I. Olier and R. Al-Kassas, *Eur. J. Pharm. Sci.*, 2021, **160**, 105765.

35 V. Dhiman and D. Pant, *J. Immunoass. Immunochem.*, 2021, **42**, 211–235.

36 L. Cristiano and M. Guagni, *Cosmet.* , 2022, 9.

37 V. Rizzi, J. Gubitosa, P. Fini, S. Nuzzo, A. Agostiano and P. Cosma, *J. Photochem. Photobiol. B Biol.*, 2021, **224**, 112309.

38 T. N. Hatuikulipi, M. Kouachi, L. E. Bouchetob and D. Naimi, *Der Pharm. Lett.*, 2016, **8**, 200–206.

39 R. Conte, *Int. J. Nano Dimens.*, 2016, **7**, 181–185.

40 C. Ellijimi, M. Ben Hammouda, H. Othman, W. Moslah, J. Jebali, H. Ben Mabrouk, M. Morjen, M. Haoues, J. Luis, N. Marrakchi, K. Essafi-Benkhadir and N. Srairi-Abid, *Biomed. Pharmacother.*, 2018, **101**, 871–880.

41 S. G. Fabi, J. L. Cohen, J. D. Peterson, M. G. Kiripolsky and M. P. Goldman, *J. Drugs Dermatol.*, 2013, **12**, 453–457.

42 M. J. Tribó-Boixareu, C. Parrado-Romero, B. Rais, E. Reyes, M. A. Vitale-Villarejo and S. González, *Cosmet. Dermatology®*, 2009, **22**, 247–252.

43 S. Greistorfer, W. Klepal, N. Cyran, A. Gugumuck, L. Rudoll, J. Suppan and J. von Byern, *Zoology*, 2017, **122**, 126–138.

44 A. S. Harti, S. D. Sulisetyawati, A. Murharyati, M. Oktariani and I. B. Wijayanti, *Int. J. Pharma Med. Biol. Sci.*, 2016, **5**, 76–80.

45 D. E. López Angulo and P. J. do Amaral Sobral, *Int. J. Biol. Macromol.*, 2016, **92**, 645–653.

46 A. Onzo, R. Pascale, M. A. Acquavia, P. Cosma, J. Gubitosa, C. Gaeta, P. Iannece, Y. Tsybin, V. Rizzi, A. Guerrieri, R. Ciriello and G. Bianco, *J. Mass Spectrom.*, 2021, **56**, e4722.

47 V. Rizzi, J. Gubitosa, P. Fini, A. Fraix, S. Sortino, A. Agostiano and P. Cosma, *Mater. Sci. Eng. C*, 2021, **119**, 111593. DOI:10.1016/j.msec.2020.111593.

48 M. F. Di Filippo, B. Albertini, L. S. Dolci, F. Bonvicini, A. Bigi, G. A. Gentilomi, N. Passerini and S. Panzavolta, *Int. J. Pharm.*, 2021, **598**, 120408.

49 Z. H. Zhang, Z. Han, X. A. Zeng, X. Y. Xiong and Y. J. Liu, *Int. J. Biol. Macromol.*, 2015, **81**, 638–643.

50 K. Ziani, J. Oses, V. Coma and J. I. Maté, *LWT - Food Sci. Technol.*, 2008, **41**, 2159–2165.

51 E. Budianto, S. P. Muthoharoh and N. M. Nizardo, *Asian J. Appl. Sci.*, 2015, 3:5. **(Asian Journal of Applied Sciences** (ISSN: 2321 – 0893) **Volume 03 – Issue 05, October 2015)**

52 Y. Duan, Y. Chen, Y. Li, C. Ni and L. Huang, *Life Res.*, 2022, **5**, 9–16.

53 A. Ryšavá, J. Vostálová and A. Rajnochová Svobodová, *Int. J. Radiat. Biol.*, 2021, **97**, 1383–1403.

54 B. Soni, E. B. Hassan, M. W. Schilling and B. Mahmoud, *Carbohydr. Polym.*, 2016, **151**, 779–789.

55 W. Chang, F. Liu, H. R. Sharif, Z. Huang, H. D. Goff and F. Zhong, *Food Hydrocoll.*, 2019, **90**, 50–61.

56 C. Branca, G. D'Angelo, C. Crupi, K. Khouzami, S. Rifici, G. Ruello and U. Wanderlingh, *Polymer (Guildf).*, 2016, **99**, 614–622.

57 I. C. Libio, R. Demori, M. F. Ferrão, M. I. Z. Lionzo and N. P. da Silveira, *Mater. Sci. Eng. C*, 2016, **67**, 115–124.

58 A. Sionkowska, *Pure Appl. Chem.*, 2015, **87**, 1075–1084.

59 D. R. Rohindra, A. V Nand and J. R. Khurma, *South Pacific J. Nat. Appl. Sci.*, 2004, **22**, 32–35.

60 J. Ostrowska-Czubenko, M. Gierszewska and M. Pieróg, *J. Polym. Res.*, 2015, **22**, 153.

61 T. Alfrey Jr., E. F. Gurnee and W. G. Lloyd, *J. Polym. Sci. Part C Polym. Symp.*, 1966, **12**, 249–261.

62 Y. Dong, Y. Ruan, H. Wang, Y. Zhao and D. Bi, *J. Appl. Polym. Sci.*, 2004, **93**, 1553–1558.

63 E. A. M. Azmy, H. E. Hashem, E. A. Mohamed and N. A. Negm, *J. Mol. Liq.*, 2019, **284**, 748–754.

64 U. G. T. M. Sampath, Y. C. Ching, C. H. Chuah, R. Singh and P.-C. Lin, *Cellulose*, 2017, **24**, 2215–2228.

65 F. E. Koc and T. G. Altıncekic, *Polym. Bull.*, 2021, **78**, 3383–3398.

66 G. F. Xu, H. M. Jing and R. X. Guo, *Appl. Mech. Mater.*, 2014, **477–478**, 1331–1335.

67 M. Doi, M. Matsumoto and Y. Hirose, *Macromolecules*, 1992, **25**, 5504–5511.

68 V. Rizzi, A. Longo, T. Placido, P. Fini, J. Gubitosa, T. Sibillano, C. Giannini, P. Semeraro, E. Franco, M. Ferrandiz and P. Cosma, *J. Appl. Polym. Sci.*, 2018, **135**, 45945. DOI:10.1002/app.45945.

69 S. Dimida, C. Demitri, V. M. De Benedictis, F. Scalera, F. Gervaso and A. Sannino, *J. Appl. Polym. Sci.*, 2015, **132**, 42256. DOI:https://doi.org/10.1002/app.42256.

70 A. Singh, S. S. Narvi, P. K. Dutta and N. D. Pandey, *Bull. Mater. Sci.*, 2006, **29**, 233–238.

71 A. Wan, Q. Xu, Y. Sun and H. Li, *J. Agric. Food Chem.*, 2013, **61**, 6921–6928.

72 V. Rizzi, I. Losito, R. Abbattista, P. Fini, A. Agostiano, T. R. I. Cataldi and P. Cosma, *J. Mol. Liq.*, 2018, **264**, 398-409. DOI:10.1016/j.molliq.2018.05.073.

DOI: 10.1039/D2TB02119F